

Photoacoustic microscopy with 2- μm transverse resolution

Geng Ku
Konstantin Maslov
Li Li
Lihong V. Wang

Washington University in St. Louis
Department of Biomedical Engineering
Optical Imaging Laboratory
Campus Box 1097
1 Brookings Drive
St. Louis, Missouri 63130

Abstract. We present a new-generation optical-resolution confocal photoacoustic microscope, consisting of a 0.25-*numerical aperture* optical microscope objective and a 75-MHz center-frequency spherically focused ultrasonic transducer. Experiments verified that this microscope has a transverse resolution of 2 μm , which is the highest to our knowledge among all photoacoustic imaging systems. *In situ* imaging of mouse ears shows the feasibility of resolving individual red blood cells in microvessels using the current system. © 2010 Society of Photo-Optical Instrumentation Engineers. [DOI: 10.1117/1.3339912]

Keywords: microscopy; photoacoustic microscopy; photoacoustic imaging; red blood cell; microcirculation.

Paper 09322SSR received Jul. 31, 2009; revised manuscript received Dec. 16, 2009; accepted for publication Dec. 17, 2009; published online Mar. 25, 2010.

1 Introduction

As an emerging high-resolution imaging modality, photoacoustic microscopy (PAM) images optically absorbing microstructures by detecting transient acoustic waves generated from laser-induced thermal-elastic expansion.¹ Current mainstream high-resolution optical imaging techniques mainly include confocal microscopy (CM), multiphoton microscopy, and optical coherence tomography (OCT). The first two tools mostly exploit fluorescence contrast and generally require introduction of exogenous dyes for imaging. OCT provides *in vivo* tissue microanatomy based on optical scattering, which carries little information about the underlying physiological functions and molecular cell biology. In contrast, PAM is directly sensitive to optical absorption, which is a quantitative measure of many physiologically important endogenous molecules (e.g., hemoglobin and melanin) as well as various widely used optical contrast agents (e.g., indocyanine green). As a result, PAM, although in its early stage, has rapidly found broad biomedical applications in mapping the morphology and function of microvasculature,^{2,3} detecting cutaneous melanoma,⁴ visualizing reporter gene expression,⁵ imaging brain function,⁶ etc. It has been predicted that PAM will join the mainstream of optical microscopy in the near future as a complement to current microscopic techniques.⁷

In traditional PAM systems, both the transverse and axial resolutions are defined by ultrasonic detection. It is difficult to achieve a transverse resolution of $<10 \mu\text{m}$ with ultrasonic focusing without compromising the imaging depth, because of the limited ultrasonic numerical aperture (NA) and the overwhelming attenuation of high-frequency ultrasound beyond 100 MHz in biological tissue. To overcome this obstacle, our group recently proposed optical-resolution PAM, whose transverse resolution is defined by a tight optical focus. Using an optical microscope objective with a NA of 0.1, 5- μm trans-

verse resolution was experimentally obtained, and microvasculature was imaged down to the single-capillary level.⁸

In this paper, we report our recent development of a new generation of optical-resolution PAM with further improved transverse resolution of $\sim 2 \mu\text{m}$. By improving the resolution, we wish to visualize individual red blood cells in microvessels and further work toward subcellular photoacoustic imaging. In the following discussion, we will refer to this new system as 2- μm PAM.

2 Methods

In the 2- μm PAM, the object is irradiated by 1.2-ns-wide laser pulses at the wavelength λ of 532 nm generated by a diode-pumped Nd:YVO₄ laser (SPOT-100-532, Elforlight). For optimal operation of the imaging system, the pulse repetition rate is controlled between 1 and 5 kHz. The imaging probe (Fig. 1), which integrates components for delivering and focusing light, sensing photoacoustic waves, and holding the object, is configured in transmission mode to minimize the resolution deterioration caused by various optical aberrations. In the first-generation optical-resolution PAM,⁸ light was delivered in free space; thus, the object had to be moved in order to form an image. In contrast, in our 2- μm PAM, a single-mode optical fiber (P1-460A-FC-2, Thorlabs) guides light to the imaging probe, which not only enables scanning the probe instead of the object to reduce motion artifacts, but also ensures that the optical beam quality is sufficient to achieve an optical diffraction limited focus. The laser pulse energy delivered through the fiber is measured to be ~ 10 nJ. The laser beam is first converged by an aspheric lens and then focused by a microscope objective (10X, Leitz Wetzlar) into the test object. The objective used here has an NA of 0.25, 2.5 times higher than the one used in the previous system, which in turn means a 2.5 time improvement in transverse resolution, in theory. The object is usually loaded on a glass slide. The generated photoacoustic wave is detected by a spherically fo-

Address all correspondence to: Lihong V. Wang, Department of Biomedical Engineering, Washington University in St. Louis, Campus Box 1097, 1 Brookings Drive, St. Louis, Missouri 63130. Tel: 314-935-6152; Fax: 314-935-7448; E-mail: lhwang@biomed.wustl.edu

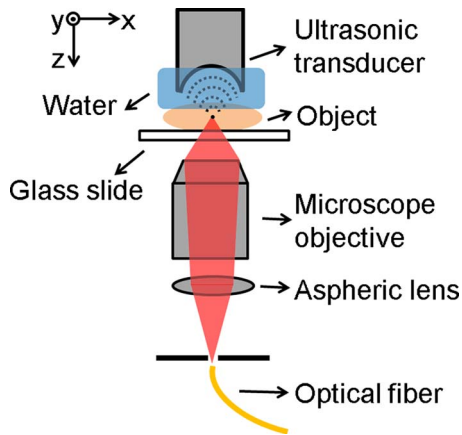


Fig. 1 Schematic of the imaging probe in the 2- μm PAM system.

cused 75-MHz ultrasonic transducer (V2022BC, Panametrics-NDT; focal length: 5 mm). The signal is first amplified by two amplifiers (ZX60-3018G and ZFL-500, Mini-Circuits) and then acquired to a computer by a 12-bit 200-MS/s high-speed digitizer (PCI-5124, National Instruments). During experiments, a drop of deionized water is applied between the sample and the transducer for efficient acoustic coupling. The optical objective and the focused transducer are prealigned confocally and coaxially. Before imaging, fine tuning is performed by maximizing the PA signal from a black calibration target.

We followed an imaging protocol similar to the one described in Ref. 9. At each transverse location, we take a time-resolved measurement of the PA waves for 1 μs . The time of arrival translates to depth along the z -axis (axial direction) through the acoustic speed in the object (e.g., 1540 m/s in soft tissue). Envelope detection is performed on each measurement to extract the PA amplitude employing the Hilbert transformation. A 3-D dataset is obtained by an x - y (transverse) raster scan of the imaging probe (x : the fast scan axis; y : the slow scan axis). Currently, it takes 12 min to acquire a volumetric dataset covering a 1×1 mm transverse area with a 1.25- μm step size. The volumetric PA amplitude is usually visualized in several ways: (i) an x - z tomogram of a cross section of the object showing depth-variant structures; (ii) an x - y tomogram representing a layer of the object at certain depth; (iii) a maximum amplitude projection (MAP) image resembling a top-down view of the object, where the maximum PA amplitude along each depth measurement is projected to the x - y plane; and (iv) various 3-D presentations.

3 Results

3.1 Evaluation of Transverse Resolution

In the 2- μm PAM, the transverse resolution is limited by the radial size of the optical focal zone. An ideal objective lens focuses a plane wave to a diffraction-limited Airy pattern, whose size is determined only by the NA and the optical wavelength.

Given the aforementioned system parameters, the blurring of a point absorber can be predicted by the full width at half maximum (FWHM) of the Airy disk, which is 1.1 μm ac-

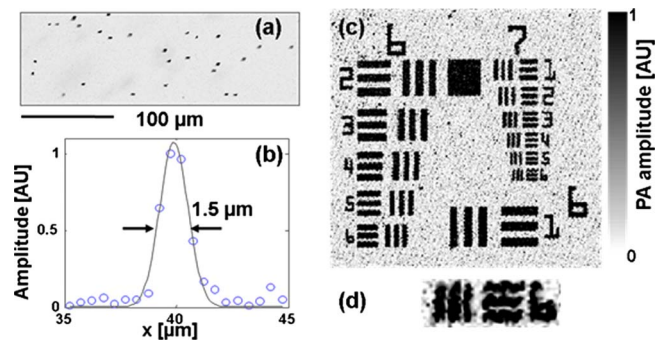


Fig. 2 Experimental validation of transverse resolution of the 2- μm PAM system. (a) MAP image of a gelatin sample mixed with nanocages. (b) Transverse spread profile of a typical nanocage. Blue circle: experimental measurements. Black line: Gaussian-fit of the experimental data. (c) MAP image of a 1951 USAF resolution test target (groups 6 and 7). (d) Close-up view of MAP image of group 7 element 6 of the test target. (Color online only.)

ording to $\text{FWHM} = 0.51\lambda/\text{NA}$. In an initial experiment, we imaged a gelatin sample mixed with gold nanocages, a promising contrast agent for photoacoustic imaging, at a low concentration. The gold nanocages have a typical edge length of 50 nm,¹⁰ and thus can be considered as point absorbers here. The MAP image shows [Fig. 2(a)] that the 2- μm PAM has the sensitivity to detect single nanocages, although their absorption is not maximized at 532 nm. The transverse profile of a typical nanocage image gives the transverse spread function of the system, and its Gaussian fit has a FWHM of 1.5 μm [Fig. 2(b)]. This value is 37% higher than the theoretical prediction. This discrepancy is probably caused by optical spherical aberration in the 1.0-mm-thick glass slide and the object. Employing a higher NA objective lens can further improve the transverse resolution, if optical spherical aberration is minimized.

In another experiment, we imaged a positive 1951 USAF resolution test target (NT38, Edmund Optics) [Fig. 2(c)]. As shown in Fig. 2(d), we were able to clearly resolve the smallest elements in this target (group 7 element 6, 228 lp/mm), where the gap between two absorptive bars is 2.2 μm wide. This result further confirms that the current system has achieved a transverse resolution of ~ 2 μm .

3.2 Evaluation of Axial Resolution

In the 2- μm PAM, axial structures are resolved by the time-resolved ultrasonic measurement. Figure 3(a) shows a typical axial spread profile of the same nanocage viewed in Fig. 2(b). Because the nanocage (~ 50 nm in size) is much smaller than axial resolution, we treat this profile as the axial point-spread function of the imaging system. The FWHM of the photoacoustic envelope was estimated to be 41 μm .

In reality, if two point absorbers are located close to each other along the axial axis, their photoacoustic signals will add in amplitude instead of in envelope. As a result, we expect to be able to distinguish the two absorbers at a separation much smaller than 41 μm . Because of the difficulty in making a phantom to test this hypothesis, we did a numerical shift-and-sum simulation. We assumed that each of the two point ab-

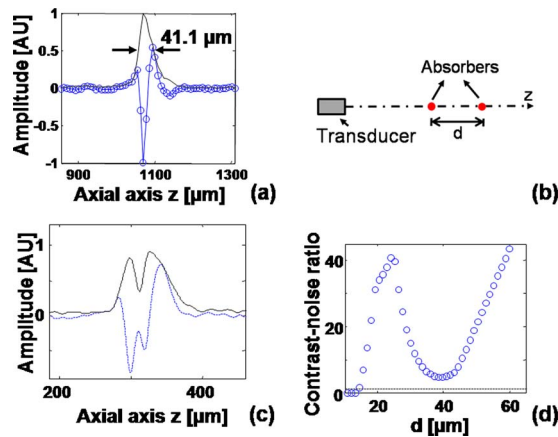
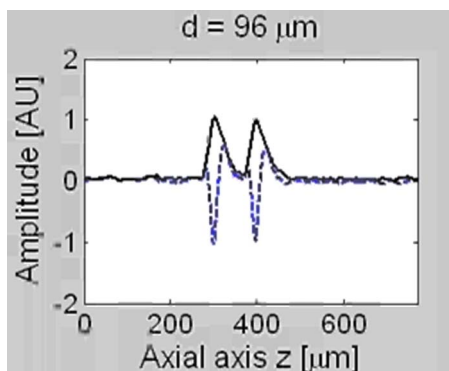


Fig. 3 Axial resolution of the 2- μm PAM system. (a) Axial spread profile of a typical nanocage. Blue line with circle: experimental measurement. Black solid line: envelope of the experimental data. (b) Configuration of numerical shift-and-sum experiment. (c) Simulated photoacoustic signal and envelope when $d=20\ \mu\text{m}$. Blue dashed line: photoacoustic signal. Black solid line: envelope of the signal. (d) CNR versus d . Blue circles: calculated CNR. Black dashed line: CNR=1. (Color online only.)

sorbers generated a photoacoustic signal shown in Fig. 3(a), and the axial distance between them was d [Fig. 3(b)]. A movie in Video 1 illustrates the evolution of the photoacoustic envelope as d decreases. Figure 3(c) proves that the photoacoustic envelope still possesses two distinct peaks representing the two absorbers when $d=20\ \mu\text{m}$. To be more quantitative, we defined a standard using the contrast-to-noise ratio (CNR). The contrast was defined as the difference in photoacoustic envelope between the smaller of the two peaks and the valley between them. The noise was defined as the standard deviation in photoacoustic envelope calculated from the experimental measurement without absorbers. The simulation shows that we can still distinguish the two absorbers with CNR=1 when $d=14\ \mu\text{m}$ [Fig. 3(d)], which is a better estimation of the axial resolution. Furthermore, with an experimentally measured photoacoustic signal from a planar absorbing object, the estimated axial resolution values using both the FWHM and shift-and-sum standards were similar to the above estimates.



Video 1 Animation showing how the measured photoacoustic signal and envelope evolve when the two absorbers move toward each other (MPEG, 1.05 MB). [URL: <http://dx.doi.org/10.1117/1.3339912.1>].

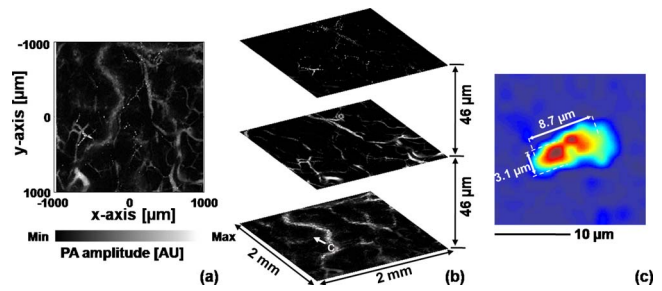
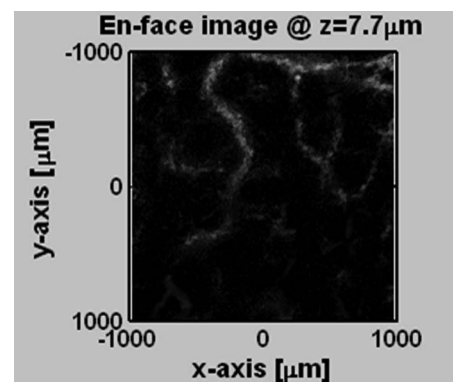


Fig. 4 Microvasculature in mouse ear imaged using the 2- μm PAM system: (a) MAP image, (b) 3-D view of three representative x - y tomograms, and (c) close-up view of a typical dot in (a).

3.3 Imaging Microvasculature in a Mouse Ear

We employed the 2- μm PAM to image an ear of a Swiss-Webster mouse (Hsd:ND4, Harlan Laboratories, Indianapolis, IN; body weight, 30 g) *in situ* shortly after death. The hair on the ear was removed, but no optical clearing agent was applied. The mouse ear is a widely used model for studying cutaneous microcirculation.¹¹ The MAP image [Fig. 4(a)] showed that the 2- μm PAM was able to depict the detailed morphology of microvasculature, similar to the first-generation optical-resolution PAM. More interestingly, we also observed a large number of “dots,” and most of them appeared to align along blood vessels. Using the three-dimensional information carried by the photoacoustic dataset, we examined transverse (x - y) tomograms at different depths [Video 2 and Fig. 4(b)]. At transverse planes out of focus, we saw smooth vasculatures. Approaching the focal plane, we saw increasing details. The dots actually appeared in the focal plane. We believe that they were red blood cells in the vessels that were located in the optical focal zone. A close-up view of a typical dot [Fig. 4(c)] showed that it had a size of $8.7 \times 3.1\ \mu\text{m}$. Because the transverse resolution is $2\ \mu\text{m}$, this observed size does match the known size of a typical red blood cell in capillaries, which is $7.5 \times 2\ \mu\text{m}$.

Finally, we tested the imaging depth of the 2- μm PAM by imaging two carbon fibers, which were placed above and below a 300- μm -thick region of an excised mouse ear close to the head. The ear was illuminated from below, and the carbon



Video 2 Animation shows the x - y tomograms of a mouse ear at different depth z (MPEG, 204 KB). [URL: <http://dx.doi.org/10.1117/1.3339912.2>].

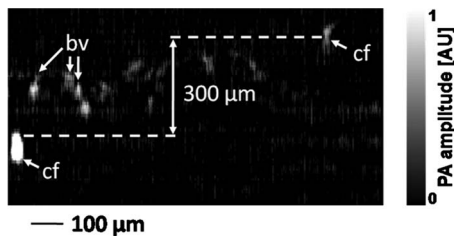


Fig. 5 x - z cross-sectional photoacoustic image of two carbon fibers placed above and below a 300- μm -thick mouse ear (cf: carbon fibers, bv: blood vessels).

fiber above the ear was placed in the focal plane. An averaged x - z cross-sectional image using 100 acquisitions is shown in Fig. 5. We were able to visualize both carbon fibers. This implies that the 2- μm PAM can penetrate deeper than 300 μm in highly scattering biological tissue such as the skin. The top fiber gives a weaker image (although in focus), because of the attenuation of ballistic photons in tissue.

4 Discussions

Existing photoacoustic methods for studying individual cells are mainly limited to a sensing technique called photoacoustic flow cytometry.¹² It monitors photoacoustic signals from individual pigmented cells at a fixed location in blood or lymph vessels and promises to detect early-stage cancer metastasis. Monitoring red blood cells flowing in microvessels usually requires a topical application of optical clearing agent. Our 2- μm PAM is the first photoacoustic imaging system to our knowledge that is able to image individual red blood cells in microvessels without optical clearing.

The 2- μm PAM uses safe radiation for photoacoustic excitation. The pulse energy was measured to be 10 nJ at the exit of the single-mode delivery fiber. If the focal plane is tuned to 100 μm below the skin, then the surface optical fluence is calculated to be $<0.5 \text{ mJ}/\text{cm}^2$, almost three orders of magnitude less than the ANSI-recommended maximum permissible exposure of $20 \text{ mJ}/\text{cm}^2$ for visible light.¹³ We have not observed any photodamage in biological samples for a prolonged period after experiments. In a clear medium, the peak fluence at the focus could reach $300 \text{ mJ}/\text{cm}^2$. A similar optical fluence at 530 nm was used *in vivo* in Ref. 12, and was also reported not to cause notable cell damage.

The present 2- μm PAM has a maximum imaging speed of ~ 1 fps, which is mainly limited by the slow mechanical scanning of the imaging probe. The red blood cells flow at a speed up to 1 mm/s in capillaries. Thus, higher imaging speed is necessary in order to follow flowing individual red blood cells *in vivo*. Potential solutions to this problem include but are not limited to (i) galvanometer scanning the optical focal spot within the broader focal zone of a single-element transducer¹⁴ and (ii) combining galvanometer scanning of light and fast ultrasonic detection using transducer array technology.

Different from acoustic-resolution PAM,² optical-resolution PAM, including the present 2- μm PAM, relies on optical focusing to achieve improved lateral resolution and works in the optical ballistic regime. Here, we briefly compare optical-resolution PAM with other existing commercial three-dimensional ballistic optical microscopy, which mainly

include CM, two-photon microscopy (TPM), and OCT. First, the amplitude of the lateral point spread function (PSF) is proportional to the optical intensity distribution at the focus in optical-resolution PAM and OCT, while the amplitude of the lateral PSF in CM and TPM is proportional to the square of the optical intensity distribution.^{15,16} As a result, if the same excitation wavelength and objective NA are used, the lateral resolution of optical-resolution PAM is the same as that of OCT and ~ 1.4 times that of CM and TPM. However, to excite the same fluorophore, TPM must use a wavelength twice as long as CM does. In this case, the lateral resolution of TPM is ~ 1.4 times that of CM. Second, CM and TPM generally require introduction of exogenous fluorescent contrast agents for *in vivo* imaging, which may not only disturb native physiological environment but also limit the frequency of longitudinal studies. OCT mainly exploits the optical scattering contrast. Thus, optical-resolution PAM complements existing techniques by noninvasively investigating physiological functions associated with endogenous chromophores, such as hemoglobin and melanin.

The axial resolution of current optical-resolution PAM is mainly limited by the acoustic-detection bandwidth, and it is an order of magnitude worse than optically defined lateral resolution in the present 2- μm PAM system. We can improve the axial resolution by using a higher-frequency ultrasonic transducer with a broader detection bandwidth, at the cost of penetration due to acoustic attenuation. Also, variation in the acoustic speed in tissue may deteriorate the axial resolution. Fortunately, the speed of sound is relatively constant in most soft tissue. For example, the difference between acoustic speeds in epidermis and dermis is $\sim 3\%$.¹⁷

5 Conclusion

In summary, we have developed a new generation of optical-resolution PAM that has an unprecedented transverse resolution of $\sim 2 \mu\text{m}$. The axial resolution was estimated to be $\sim 14 \mu\text{m}$, and the maximum penetration depth was tested to be at least $\sim 300 \mu\text{m}$ in highly scattering biological tissue. Preliminary *in situ* studies on a mouse ear showed that it is feasible to visualize individual red blood cells in microvessels. The transverse resolution can be improved by employing a higher NA objective lens and carefully controlling optical aberrations. With future improvements in imaging speed, we expect that this new imaging technology will find broad *in vivo* applications in quantifying capillary flow, oxygenation, and potentially the metabolic rate of oxygen at the single-cell level, and will provide new insight into microcirculation studies.

Acknowledgments

We thank Younan Xia's group for providing gold nanocages. This work was supported in part by National Institutes of Health Grants No. R01 NS46214 (BRP), No. R01 EB000712, No. R01 EB008085, and No. U54 CA136398 (NTR). L.W. has a financial interest in Microphotoacoustics, Inc. and Endra, Inc., which, however, did not support this work.

References

1. L. V. Wang, "Tutorial on photoacoustic microscopy and computed tomography," *IEEE J. Sel. Top. Quant.* **14**(1), 171–179 (2008).

2. K. Maslov, G. Stoica, and L. V. Wang, "In vivo dark-field reflection-mode photoacoustic microscopy," *Opt. Lett.* **30**(6), 625–627 (2005).
3. H. F. Zhang, K. Maslov, G. Stoica, and L. H. V. Wang, "Functional photoacoustic microscopy for high-resolution and noninvasive *in vivo* imaging," *Nat. Biotechnol.* **24**(7), 848–851 (2006).
4. J. T. Oh, M. L. Li, H. F. Zhang, K. Maslov, G. Stoica, and L. V. Wang, "Three-dimensional imaging of skin melanoma *in vivo* by dual-wavelength photoacoustic microscopy," *J. Biomed. Opt.* **11**(3), 034032 (2006).
5. L. Li, H. F. Zhang, R. J. Zemp, K. Maslov, and L. V. Wang, "Simultaneous imaging of a lacZ-marked tumor and microvasculature morphology *in vivo* by dual-wavelength photoacoustic microscopy," *J. Innov. Opt. Health Sci.* **1**(2), 207–215 (2008).
6. E. W. Stein, K. Maslov, and L. V. Wang, "Noninvasive, *in vivo* imaging of blood-oxygenation dynamics within the mouse brain using photoacoustic microscopy," *J. Biomed. Opt.* **14**(2), 020502 (2009).
7. L. V. Wang, "Prospects of photoacoustic tomography," *Med. Phys.* **35**(12), 5758–5767 (2008).
8. K. Maslov, H. F. Zhang, S. Hu, and L. V. Wang, "Optical-resolution photoacoustic microscopy for *in vivo* imaging of single capillaries," *Opt. Lett.* **33**(9), 929–931 (2008).
9. H. F. Zhang, K. Maslov, and L. H. V. Wang, "In vivo imaging of subcutaneous structures using functional photoacoustic microscopy," *Nat. Protoc.* **2**(4), 797–804 (2007).
10. X. Yang, S. E. Skrabalak, Z.-Y. Li, Y. Xia, and L. V. Wang, "Photoacoustic tomography of a rat cerebral cortex *in vivo* with Au nanocages as an optical contrast agent," *Nano Lett.* **7**(12), 3798–3802 (2007).
11. J. H. Barker, F. Hammersen, I. Bondar, E. Uhl, T. J. Galla, M. D. Menger, and K. Messmer, "The hairless mouse ear for *in vivo* studies of skin microcirculation," *Plast. Reconstr. Surg.* **83**(6), 948–959 (1989).
12. V. P. Zharov, E. I. Galanzha, E. V. Shashkov, N. G. Khlebtsov, and V. V. Tuchin, "In vivo photoacoustic flow cytometry for monitoring of circulating single cancer cells and contrast agents," *Opt. Lett.* **31**(25), 3623–3625 (2006).
13. Laser Institute of America, "American National Standard for Safe Use of Lasers ANSI Z136.1-2000," American National Standards Institute, Inc. (2000).
14. Z. X. Xie, S. L. Jiao, H. F. Zhang, and C. A. Puliafito, "Laser-scanning optical-resolution photoacoustic microscopy," *Opt. Lett.* **34**(12), 1771–1773 (2009).
15. L. V. Wang and H. Wu, "Ballistic imaging and microscopy," Chap. 8 in *Biomedical Optics: Principles and Imaging*, Wiley, Hoboken, NJ (2007).
16. L. V. Wang and H. Wu, "Optical coherence tomography," Chap. 9 in *Biomedical Optics: Principles and Imaging*, Wiley, Hoboken, NJ (2007).
17. C. M. Moran, N. L. Bush, and J. C. Bamber, "Ultrasonic Propagation Properties of Excised Human Skin," *Ultrasound Med. Biol.* **21**(9), 1177–1190 (1995).